JMEPEG (2021) 30:1030–1038
https://doi.org/10.1007/s11665-020-05420-6

1059-9495/$19.00

Microstructure and Mechanical Properties of an Austenitic Heat-Resistant Steel after Service at 570 °C and 25.4 MPa for 18 Years

Xu Yang, Chengwei Yu, Xisheng Yang, Kai Yan, Gong Qian, Baochen Wang, Wei Yan, and Xianbo Shi

Submitted: 27 May 2020 / Revised: 30 November 2020 / Accepted: 12 December 2020 / Published online: 5 January 2021

Microstructure and mechanical properties of an austenitic heat-resistant steel (12Cr18Ni12Ti) serviced in a supercritical power plant at 570 °C/25.4 MPa for 160,000 h were investigated. The results show that the hardness and the tensile strength did not decrease; however, the impact toughness was remarkably reduced. The TiC precipitate shows excellent thermostability; for example, it hardly grew up, and no big $M_{23}C_6$ carbides were found. However, large Fe, Cr-rich σ-phase was doomed to precipitate along grain boundary, which should be responsible for the reduced toughness. The growth of σ-phase was observed to have an interaction with the preexisted carbides.

Keywords 12Cr18Ni12Ti, austenitic stainless steel, long-term service, mechanical properties, microstructure

1. Introduction

Austenite stainless steels are the most widely used in power plants due to the excellent creep strength, high resistance to oxidation and mature manufacturing process (Ref 1-3). Such austenite stainless steels generally include S304, S310, S316, S316L, and so on. Among them, S316 is the most popular and typical one, with excellent mechanical properties and oxidation resistance. In order to improve the intergranular corrosion resistance, strong carbide forming elements such as Ti and Nb were introduced in S316 steels and many modified steels have been developed (Ref 2, 3).

In the present research, the experimental steel (12Cr18Ni12-Ti) is such kind of modified S316 steel by adding the element of Ti. Since Ti has a very strong bonding force with C so as to get TiC precipitates, Cr has little chance to form carbides with C at grain boundaries, and thus, the intergranular corrosion resistance could be improved (Ref 4-6). Besides, the TiC precipitates are beneficial to improve creep strength (Ref 4, 5, 7). Therefore, compared with S316 steel, 12Cr18Ni12Ti steel has better intergranular corrosion resistance and higher creep strength (Ref 4-7).

However, the steam tubes in power plants made of such stainless steels usually have to face extreme conditions such as high temperature, stress and corrosion. During exposure under these special conditions, steels are doomed to undergo microstructural evolution, leading to mechanical properties degeneration (Ref 8-10). Such microstructural evolution during high-temperature and long-term service in austenite heat-resistant steels mainly involves the following aspects: (1) growth of austenite grain size; (2) ripening of precipitates such as carbides and nitrides; and (3) formation and growth of σ-phase (Ref 8-15).

To safe use of such austenite heat-resistant steel exposing in service environment in power plants, the prediction of microstructural evolution and its influence on mechanical properties prior to use is of great significance to the power industrial practice. However, this prediction is usually performed by high-temperature short-term experiment in the laboratory. In fact, such experiment is difficult in reflecting the real service environment. In the present work, the microstructure and mechanical properties of an austenitic heat-resistant steel (12Cr18Ni12Ti) serviced in a real service condition of 570 °C/25.4 MPa for more than 18 years (160,000 h) were studied. Up to now, very few responses of microstructure and mechanical property after such long-term high-temperature exposure have been reported on the 12Cr18Ni12Ti steel. This type of data is difficult to obtain, especially in the real service status. The data can not only provide a meaningful reference for the safe use of this steel but also are invaluable to understanding the long-term performance of materials in realistic conditions.

2. Materials and Methods

The as-received trial materials were obtained from a steam tube in a super critical power plant came from Tianjin Guohua Panshan Power Generation Co., Ltd. The tube has served at 570 °C/25.4 MPa for more than 18 years (160,000 h). The initial material which was set up 18 years ago was compared. The chemical composition of the experimental steel is shown in Table 1. After such a long-term service at 570 °C, the changes in microstructure and mechanical properties are of great

Xu Yang, Xisheng Yang, Kai Yan, and **Gong Qian**, China Special Equipment Inspection and Research Institute, Beijing 100029, China; **Chengwei Yu**, Tianjin Guohua Panshan Power Generation Co., Ltd, Tianjin 301900, China; **Baochen Wang**, Guohua Electric Power Branch of China Shenhua Energy Co., Ltd, Beijing 100025, China; and **Wei Yan** and **Xianbo Shi**, Institute of Metal Research, Chinese Academy of Sciences, Shenyang 110016 Liaoning, China. Contact e-mail: 592782553@qq.com.

importance. Therefore, the grain size of the steel was firstly investigated under the optical microscope by statistical image analysis. For more details, the scanning electron microscope (SEM) with energy-dispersive x-ray (EDX) analysis was employed to reveal the precipitates such as carbides and σ-phase along grain boundaries. The interaction between precipitates along the grain boundaries was also studied under transition electron microscope (TEM).

Hardness measurements were conducted on polished surface of the trial tube using a UH3001 Brinell hardness tester with a load of 187.5 kgf for 13 s, and the average value from 3 different measurements is recorded. Tensile samples with diameter of 5 mm and gauge length of 25 mm machined from pillars cut out from the trial tube. They were suffered from tensile test on an AG-Xplus 50 kN tensile machine. To obtain much more data, the tensile tests were carried out not only at room temperature and real service temperature (570 °C), but also 540 and 600 °C compared. To assure the reliability of the tensile results, 3 samples were tested to obtain the average value. The Charpy V-notch samples with the dimension of $10 \times 10 \times 55$ mm^3 and notch depth of 2 mm machined from pillars from the trial tube were subjected to impact test on a RKP-450 Charpy impact machine. The average of 5 results was recorded.

3. Results

3.1 Microstructure

3.1.1 Austenite Grain Size. The microstructure of the initial material and the steam tube serviced at 570 °C for 160,000 h is shown in Fig. 1. The original grain boundaries are clearly identified, and the grain size ranges around 50-120 μm. In addition, inside the grains are numerous parallel deformation twins. It is clear that the austenite grain size is not uniform after serviced for 160,000 h. The large grains are around 150 μm, while the small grains are around 50 μm. However, the number of small grains is bigger than that of large ones. Therefore, the average grain size is around 120 μm, as shown in Fig. 1. It indicates that under the long-term high-temperature condition, austenite grain is still under the control of thermodynamics and reaching for equilibrium, during which the growth of the big grains was through sacrificing the small ones.

Table 1 Chemical compositions of the 12Cr18Ni12Ti steam tube (wt.%)

C	Si	Mn	S	P	Cr	Ni	Ti
0.077	0.43	1.05	0.0099	0.028	17.39	11.28	0.64

3.1.2 Precipitates. *TiC particles* The TiC particles in the initial 12Cr18Ni12Ti steel are shown in Fig. 2. Two kinds of TiC particles are observed. One is around 2-4 μm in size, another is nano-sized. The larger ones are believed to be the primary TiC, which are formed during solidification, while the nano-sized ones are secondary TiC. The TiC particles in the 12Cr18Ni12Ti steam tube after such a long-term high-temperature service are shown in Fig. 3. Also, two categories of TiC particles are observed. The first category is black precipitates as large as 2 μm which are indicated by black arrows in Fig. 3(a) and (b). They are distributed either inside the grain (Fig. 3a) or at the grain boundary (Fig. 3b). The second category is white particles with small sizes of around 750 nm, as marked by white arrows in Fig. 3(a) and (b). The corresponding EDX results of such two categories of TiC particles are shown in Fig. 3(c) and (d), respectively. The size of TiC particles is almost no coarsening. In addition, it was not obviously increased compared with another Ti modified S316 steel, which serviced at 545 °C/25.5 MPa for 13,600 h (Ref 16). Therefore, it could be inferred that the TiC particles are very thermally stable and barely grow even after such a long-term exposure.

$M_{23}C_6$ Particles As shown in Fig. 2, there are almost no $M_{23}C_6$ particles in the microstructure of the initial material because Ti has a very strong bonding force with C; as a result, $M_{23}C_6$ cannot be formed in a short time. It is clearly shown in Fig. 4(a) and (b) that $M_{23}C_6$ particles were mainly distributed along grain boundaries after service for 18 years. Even the large $M_{23}C_6$ particles are with the fine size of around 200 nm, as shown in Fig. 4(b), which means that $M_{23}C_6$ particles have a very small ripening rate at 570 °C in this steel. The EPMA results in Fig. 4(c) show that Ti was also segregated in $M_{23}C_6$ particles, which enhances the thermostability of such carbides.

σ-phase As mentioned above, due to the high content of chromium in the 12Cr18Ni12Ti steel, σ-phase will come into being during the long-term high-temperature exposure. As shown in Fig. 5, the σ-phases formed during long-term

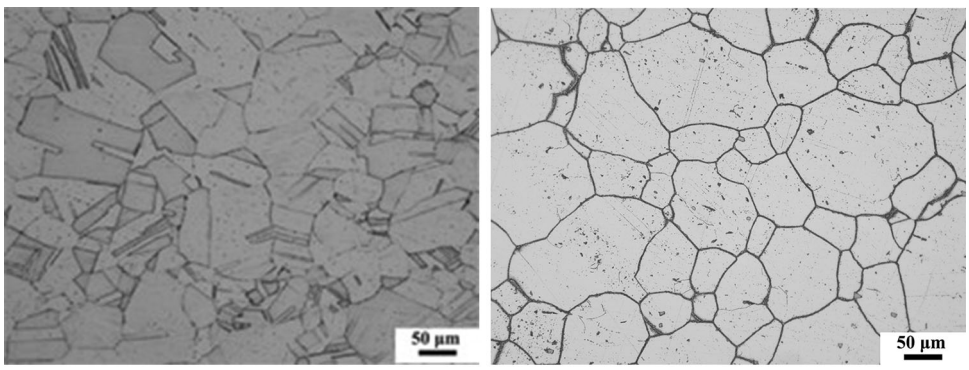

Fig. 1 The microstructure of initial 12Cr18Ni12Ti steel (a) and the austenite grain size of the 12Cr18Ni12Ti steam tube (b)

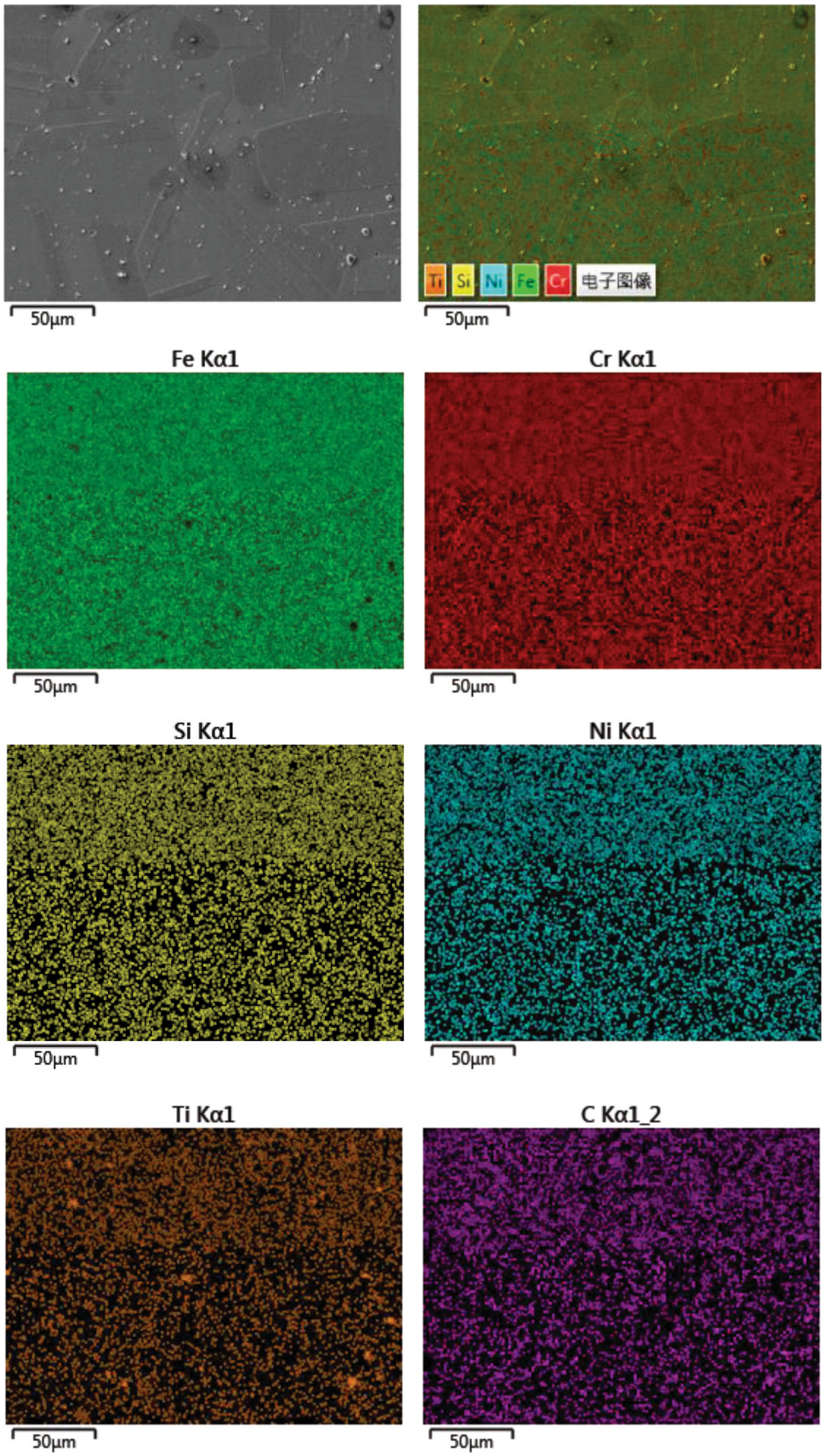

Fig. 2 The TiC particles in the initial 12Cr18Ni12Ti steel

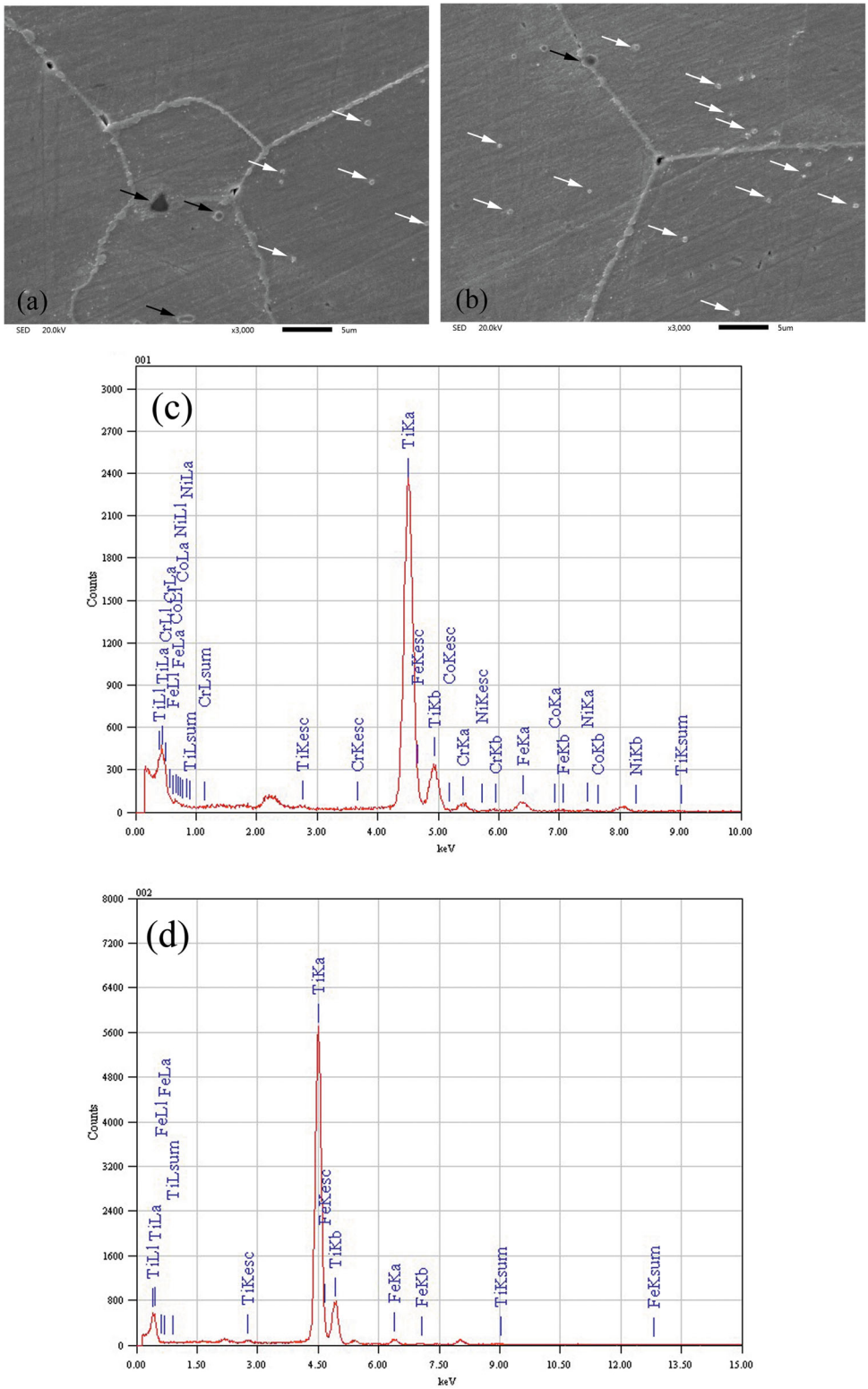

Fig. 3 (a) and (b) Morphologies with (c) and (d) EDX analysis of TiC particles in the 12Cr18Ni12Ti steam tube (black arrows show large TiC particles, and white arrows show small TiC particles)

exposure at 570 °C were distributed along grain boundaries. Some are in the shape of pearls and clustered along grain boundaries like a section of necklace, as designated by white arrows in Fig. 5(a). Some are in the shape of short bar, as marked by black arrows in Fig. 5. The others are isolated at the connection points of adjacent grains, as indicated by red arrows in Fig. 5. It seems that it is easier for σ-phase to nucleate at the connection points of grain boundaries. Adjacent σ-phase particles might grow up and get connected with each other and then give a bar-like shape.

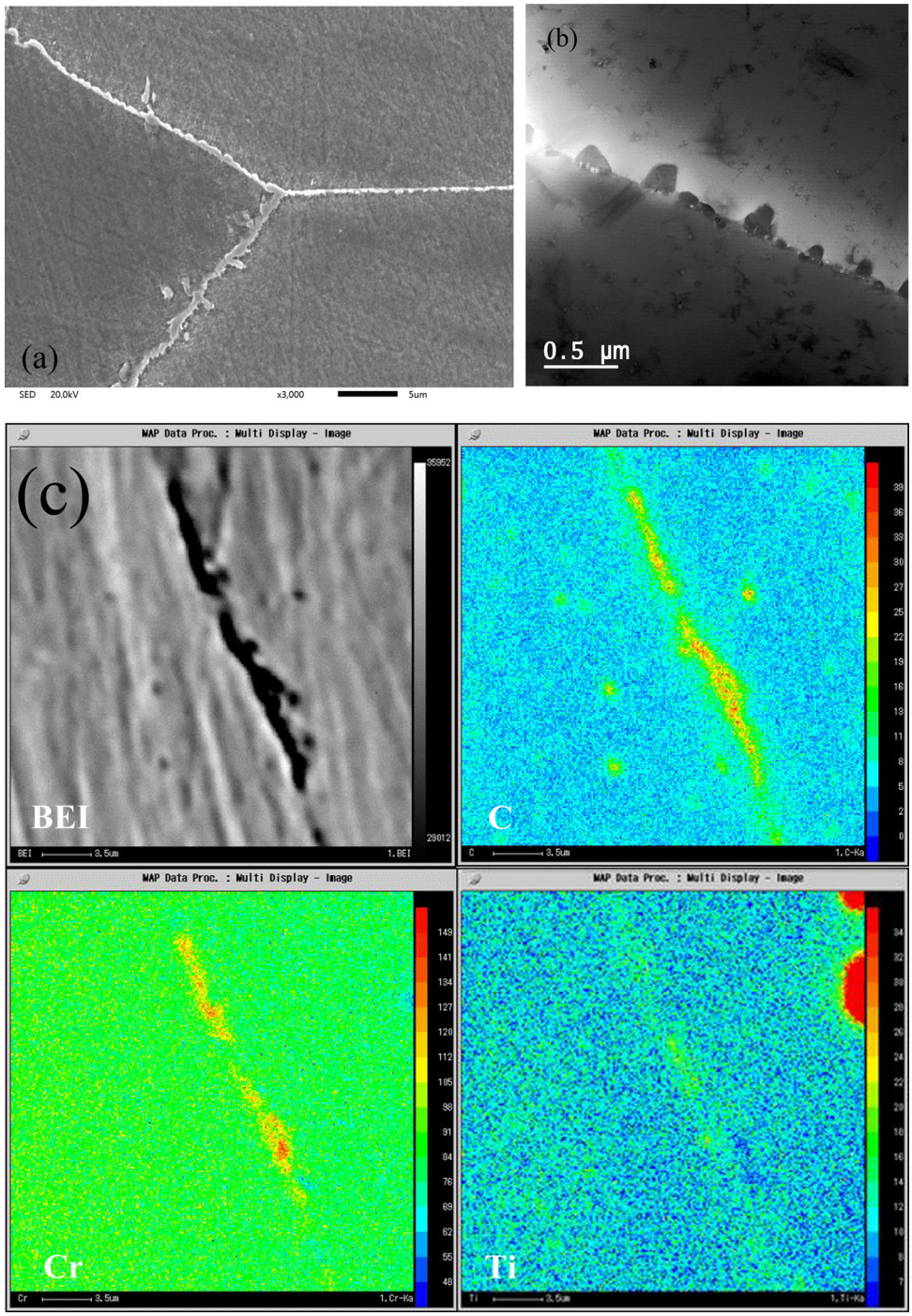

Fig. 4 Morphologies of (a) SEM, (b) TEM and (c) EPMA results of $Cr_{23}C_6$ particles

The TEM images showing the details of σ-phase are presented in Fig. 6 and 7. It is noticed that σ-phase is with very few dislocations, as shown in Fig. 6(a), (b), (c) and 7(a), (b). Only several dislocations are presented in the σ-phase particles in Fig. 6(d), but all the three isolated particles in Fig. 6 are very clean inside. The bar-like σ-phase in Fig. 6(a) seems to be composed of three smaller particles, as indicated by black arrows. Based on the SEM images and the TEM images, it could be suspected that the bar-like σ-phase is coming into the bar shape through merging of adjacent σ-phase particles.

It is interesting here to observe the interaction between σ-phase and precipitates, as shown in Fig. 7. The bar-like σ-phase identified in Fig. 7(c) is swallowing a large particle which is marked by black arrows in Fig. 7(a). This large particle was identified as $M_{23}C_6$ carbide in Fig. 7(d). There are three other small particles lying in the middle of σ-phase, as noticed by white arrows in Fig. 7(a). Another large particle marked by a red arrow in Fig. 7(a) was still lying at the left end top of the σ-phase, kissing this σ-phase. It is worth noticing that these precipitates are distributed not only in line but also right in the

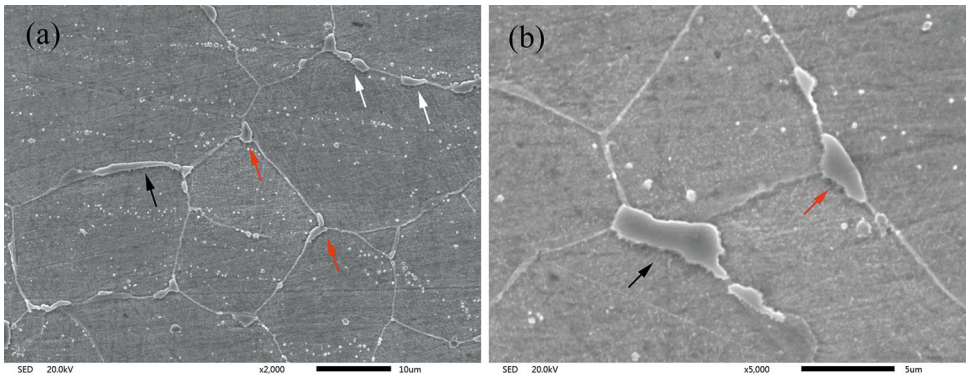

Fig. 5 SEM images showing the morphology of σ-phase: (a) macrograph; (b) micrograph (white arrows show pearls-like σ-phase, black arrows show short-bar σ-phase and red arrows show isolated σ-phase)

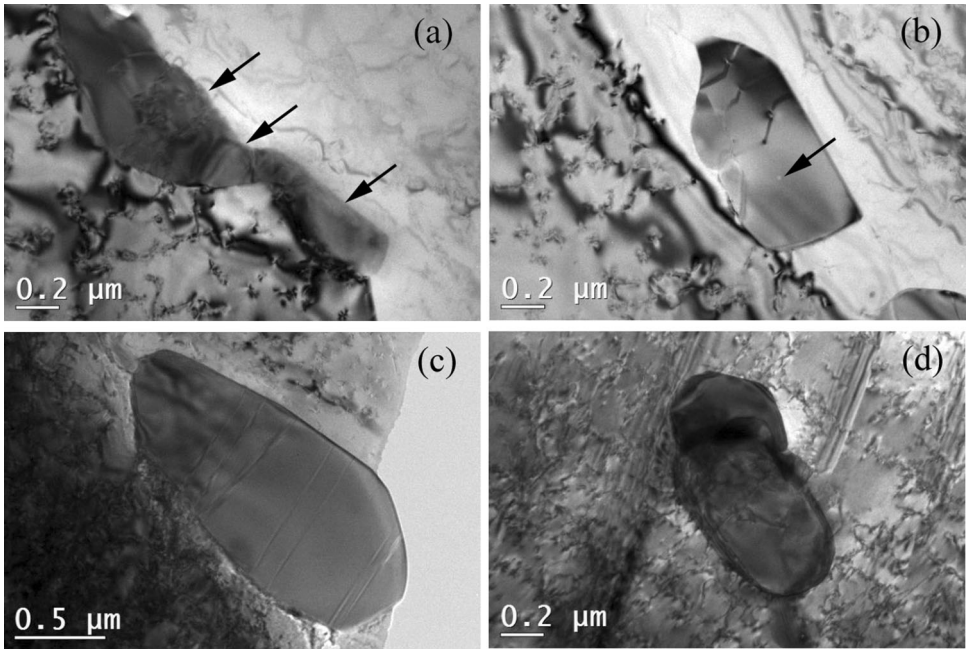

Fig. 6 TEM images showing the morphology of σ-phase

middle of this σ-phase. The line-distributed precipitates are embodied the original location of austenite grain boundaries. So, it means that the σ-phase was growing up without leaning to either side, which is in good consistence with the SEM images of σ-phase in Fig. 5; for example, σ-phase totally covered at grain boundaries, without tending to one side or the other. Figure 7(b) gives the high magnification of the interaction between σ-phase and the large particle. It is clear that the boundary of σ-phase is crossing the large $M_{23}C_6$ particle. The two sides of the boundary are bowing out and reaching for each other, and will finally get emerged when the large particle is swallowed. There is also a small precipitate swallowed by the σ-phase in Fig. 6(b), as marked by a black arrow.

3.2 Mechanical Properties

Table 2 shows the mechanical properties of the initial material and steel after service at 570 °C for 160,000 h. It is very impressive that even after such a long-term high-temperature exposure, the mechanical properties of 12Cr18Ni12Ti steel have not obviously deteriorated except the Charpy impact energy. As shown in Table 2, the steel still exhibited normal hardness, high strength and good ductility, which are comparable to the level of the as-manufactured state (Ref 17). However, as to the Charpy impact energy, it has been decreased to 87 J, far lower than the original level of above 190 J (Ref 18). But this toughness storage is still sufficiently for the safety of steam tubes (Ref 19). In addition, 12Cr18Ni12Ti steel after service at 570 °C/25.4 MPa for 160,000 h is still showing a normally decrease in strength with increasing temperature from RT to 540, 570 and 600 °C. Based on the above mechanical properties, it is claimed that the 12Cr18Ni12Ti steel is excellent in high-temperature long-term performance.

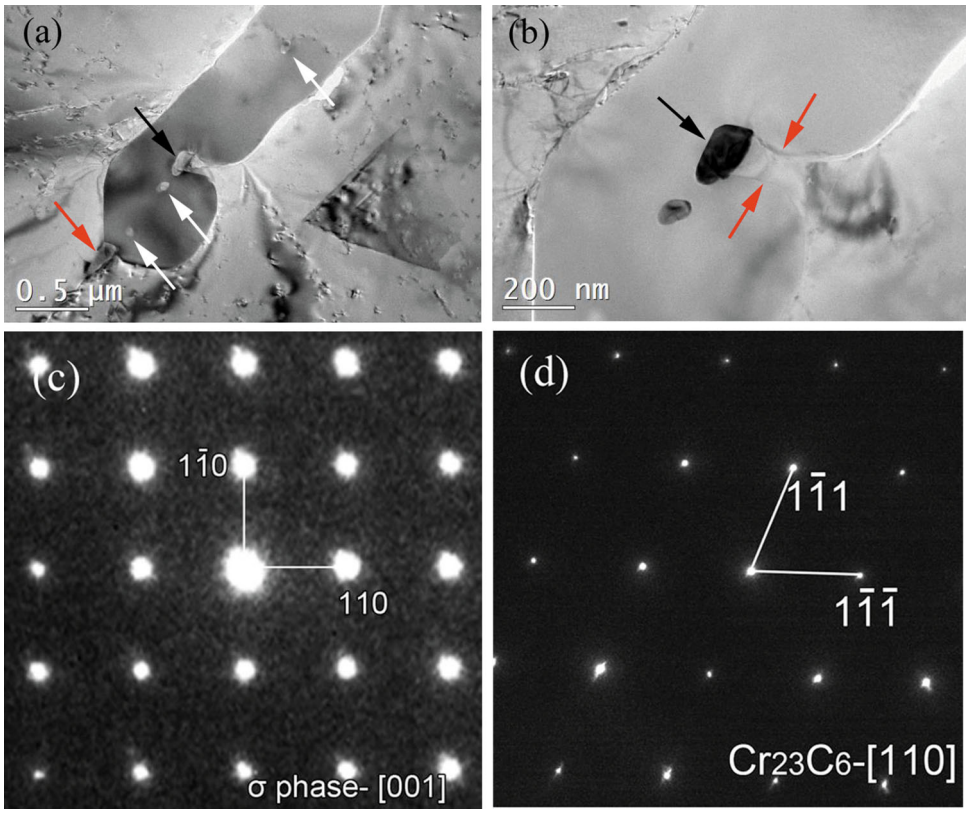

Fig. 7 (a) and (b) TEM images showing the interaction between σ-phase and precipitates, (c) is the diffraction pattern of the bar-like σ-phase, (d) is the diffraction pattern of $Cr_{23}C_6$ carbide, which is the large particle marked by black arrows

Table 2 Mechanical properties of the initial steel and steel after service at 570 °C for 160,000 h

	Temperature, °C	Yield strength, MPa	Ultimate tensile strength, MPa	Elongation, %	Area reduction, %	Charpy impact energy, J	Hardness HB
The initial steel	RT	247	608	60	76	196	159
As-received steel	RT	308	649	49	61	87	163
	540	254	436	30	66	…	…
	570	248	429	29	67	…	…
	600	235	412	30	66	…	…
GOST 7350-77 standard	RT	≥ 235	≥ 530	≥ 38	…	…	…

4. Discussion

4.1 Stability of Precipitates

It is evident that TiC particles have the highest thermostability among the precipitates in the investigated 12Cr18Ni12Ti steel. They are almost immune to such a high-temperature long-term exposure. The large TiC precipitates could be existed before the steam tubes made of 12Cr18Ni12Ti steel was carried into practice and always are accepted as the primary carbides. However, those small TiC particles in Fig. 3 are mainly the secondary carbides which were formed during hot processing or heat treatment. Anyway, two categories of TiC particles have a common contribution of fixing carbon. But of course, the small TiC particles could also give a second benefit to creep strength by precipitation hardening.

Just because Ti has a stronger combination with carbon, only small amount of carbon was left for Cr to form $M_{23}C_6$ carbides, which has resulted in two advantages: (1) $M_{23}C_6$ carbides are very fine and not in a great amount; (2) $M_{23}C_6$ carbides are with slow ripening rate, around 200 nm even after exposure for more than 18 years (160,000 h) at 570 °C (Fig. 4b). That is to say that $M_{23}C_6$ carbides in 12Cr18Ni12Ti steel also show a very good thermostability due to the synergistic effect of Ti.

The above might be one of the reasons that in the Ti-alloyed 12Cr18Ni12Ti steel $M_{23}C_6$ carbides have a good thermostability. Besides the indirect advantages of forming TiC particles and suppressing the formation of $M_{23}C_6$ carbides, Ti still has another benefit. As shown in the EPMA results in Fig. 4(c), it was revealed that Ti segregates in $M_{23}C_6$ particles, which will directly modify the physical characteristics of $M_{23}C_6$ carbides and improve their thermostability.

4.2 r-Phase Interacts with Precipitates

σ-phase particles are formed during high-temperature long-term exposure, which are very critical to the degenerated mechanical properties since they are always present as large size particles. Therefore, they should be paid enough attention to. In the present study, one thing is for sure that σ-phase particles are growing up right on grain boundaries without leaning to either side in 12Cr18Ni12Ti steel; the other thing is that σ-phase swallows the precipitates distributed at grain boundaries such as $M_{23}C_6$ carbides by boundary crossing mechanism. However, one thing must be emphasized that not all σ-phase particles were observed to contain precipitates such as $M_{23}C_6$ carbides in the middle. In the present results, only in the σ-phase in Fig. 6(b) and 7 the swallowed precipitates were observed. The other observed σ-phase particles are not containing precipitates inside, as clean as the one in Fig. 6(c). Since it is hard for σ-phase particles to find a section of grain boundary without precipitates to nucleate and grow up, it gives an interesting speculation that after the first process of swallowing, it is possible that there might be another process of digestion, namely the precipitates in σ-phase might eventually get dissolved and disappeared. That might be a possible reason for the cleanness in many σ-phase particles. More work would be done to dig deeper in it.

4.3 Reduced Toughness

After the investigation of microstructural evolution in 12Cr18Ni12Ti steel after service at 570 °C for 160,000 h, a consequent indication is turning out that the newly formed σ-phase along grain boundaries should be responsible for the reduced toughness, taking the following reasons into consideration. At first, the TiC precipitates are large and usually reported to trigger cleavage fractures and do harm to toughness (Ref 7), but they are not in a great number in the present 12Cr18Ni12Ti steel, and the austenite heat-resistant steels have high ductility and a high tolerance of large inclusions. In addition, even with such large TiC precipitates, the as-manufactured 12Cr18Ni12Ti steel could possess high impact energy higher than 190 J. Therefore, these TiC precipitates are not related to the reduced toughness. Those little TiC particles of around several hundred microns are too small to damage the toughness, but benefit creep strength. Secondly, $M_{23}C_6$ carbides are distributed along the austenite grain boundaries, but they are also very fine, around 200 nm (Fig. 4). Even if they brought some reduction to toughness, it should not be the main one.

However, when it comes to σ-phase, the above considered aspects are turning against it. First, it presents as inclusions as large as 2-10 μm. Second, they are located at the grain boundaries. It should be noticed that TiC particles could also reach the size of 5 μm, but their locations are random (Fig. 3a and b) and their number density is much lower than σ-phase, as shown in Fig. 5(a). Thirdly, σ-phase itself is very hard, brittle and unmatched with the matrix during deformation, which facilitates cracking (Ref 20-22). Therefore, it is reasonable that σ-phase should be responsible for the reduced Charpy impact toughness.

5. Conclusions

As a component of steam tubes in power plants, Ti-alloyed 12Cr18Ni12Ti steel has been investigated after service in a real environment of 570 °C/25.4 MPa for more than 18 years (160,000 h) from the aspects of microstructure and mechanical properties. The following conclusions could be reached:

1. 12Cr18Ni12Ti steel still possesses nice mechanical properties, only with reduced impact toughness, but it is still enough for engineering practice.
2. TiC particles are presented in two categories in 12Cr18Ni12Ti steel. One is a few big inclusions as large as several microns; the other is quite a lot small particles of 700 nm. TiC particles are very thermally stable, nearly no changes in size at all.
3. $M_{23}C_6$ carbides have also presented a good thermostability due to the synergistic effect of Ti.
4. σ-phase grows up right at grain boundaries without leaning to either side, during which it swallows precipitates distributed along grain boundaries.
5. σ-phase formed during high-temperature long-term exposure is believed to be responsible for the reduced toughness of 12Cr18Ni12Ti steel.

Conflict of interest

The authors declare that there is no conflict of interests regarding the publication of this paper.

References

1. G. Chai, M. Boström, M. Olaison, and U. Forsberg, Creep and LCF Behaviors of Newly Developed Advanced Heat Resistant Austenitic Stainless Steel for A-USC, *Procedia Eng.*, 2013, **55**, p 232–239
2. R. Viswanathan, J. Sarver, and J.M. Tanzosh, Boiler Materials for Ultra-Supercritical Coal Powerplants: Steamside Oxidation, *J. Mater. Eng. Perform.*, 2006, **15**(3), p 255–274
3. R. Viswanathan and W. Bakker, Materials for Ultrasupercritical Coal Power Plants: Turbine Materials—Part II, *J. Mater. Eng. Perform.*, 2001, **10**(1), p 81–95
4. K.S. Min and S.W. Nam, Correlation Between Characteristics of Grain Boundary Carbides and Creep–Fatigue Properties in AISI, 321 Stainless Steel, *J. Nucl. Mater.*, 2003, **322**, p 91–97
5. A. Pardo, M.C. Merino, A.E. Coy, F. Viejo, M. Carboneras, and R. Arrabal, Influence of Ti, C and N Concentration on the Intergranular

Corrosion Behaviour of AISI, 316Ti and 321 Stainless Steels, *Acta Mater.*, 2007, **55**(7), p 2239–2251
6. K.H. Lo, C.H. Shek, and J.K.L. Lai, Recent Developments in Stainless Steels, *Mater. Sci. Eng. R.*, 2009, **65**(4–6), p 39–104
7. K.S. Min, K.J. Kim, and S.W. Nam, Investigation of the Effect of the Types and Densities of Grain Boundary Carbides on Grain Boundary Cavitation Resistance of AISI, 321 Stainless Steel Under Creep–Fatigue Interaction, *J. Alloys Compd.*, 2004, **370**, p 223–229
8. Y.S. Ji, J. Park, S.Y. Lee, J.W. Kim, S.M. Lee, J. Nam, B. Hwang, J.Y. Suh, and J.H. Shim, Long-Term Evolution of σ-Phase in 304H Austenitic Stainless Steel: Experimental and Computational Investigation, *Mater. Charact.*, 2017, **128**, p 23–29
9. S.M. Dubiel, Sigma Phase: One of the Main Reasons for Deterioration of Stainless Steels Properties, *Hyperfine Interact.*, 2009, **189**, p 53–61
10. C. Barbosa, J.L. Nascimento, I.M.V. Caminha, and I.C. Abud, Microstructural Aspects of the Failure Analysis of Nickel Base Superalloys Components, *Eng. Fail. Anal.*, 2005, **12**, p 348–361
11. R.K. Wang, Q.W. Zhou, Z.J. Zheng, and Y. Gao, The Negative Effect of High-Intensity Shot-Peening on the Intergranularcorrosion Behavior of the Super304H Austenitic Stainless Steel, *Corros. Sci.*, 2018, **143**, p 390–402
12. E.O. Hall and S.H. Algie, The Sigma Phase, *Metall. Rev.*, 1966, **11**(1), p 61–88
13. A. Bahrami, A. Ashrafi, S.M. Rafiaei, and M.Y. Mehr, Sigma Phase-Induced Failure of AISI, 310 Stainless Steel Radiant Tubes, *Eng. Fail. Anal.*, 2017, **82**, p 56–63
14. M. Schwind, J. Källqvist, J.-O. Nilsson, J. Ågren, and H.-O. Andren, σ-Phase Precipitation in Stabilized Austenitic Stainless Steels, *Acta Mater.*, 2000, **48**, p 2473–2481
15. Q.W. Zhou, J.W. Liu, and Y. Gao, An Insight into Oversaturated Deformation-Induced Sigma Precipitationin Super304H Austenitic Stainless Steel, *Mater. Des.*, 2019, **181**, p 108056
16. C. Che, W.Y. Dou, and X.Z. Chen, Burst Failure Analysis of High Temperature Superheater in Supercritical Boiler, *Heat Treat. Met.*, 2015, **40**, p 189–193 ((in Chinese))
17. W.C. Li, *Failure Analysis of Machinery and Equipment*, Metallurgical Industry Press, Beijing, 2008, p 254–255
18. K. Guan, X.D. Xu, H. Xu, and Z.W. Wang, Effect of Aging at 700 °C on Precipitation and Toughness of AISI, 321 and AISI, 347 Austenitic Stainless Steel Welds, *Nucl. Eng. Des.*, 2005, **235**, p 2485–2494
19. Boiler Safety Technical Supervision Administration Regulation, TSG G0001-2012. AQSIQ (2012)
20. B.S. Dutt, G. Sasikala, G. Shanthi, S. Venugopal, M.N. Babu, P.K. Parida, and A.K. Bhaduri, Mechanical Behaviour of SS 316 (N) Weld after Long Term Exposure to Service Temperatures, *Procedia Eng.*, 2011, **10**, p 2725–2730
21. J. Anburaj, S.S. Mohamed Nazirudeen, R. Narayanan, B. Anandavel, and A. Chandrasekar, Ageing of Forged Superaustenitic Stainless Steel: Precipitate Phases and Mechanical Properties, *Mater. Sci. Eng. A*, 2012, **535**, p 99–107
22. R.L. Plaut, H. Clara, D.M. Escriba, P.R. Rios, and A.F. Padilha, A Short Review on Wrought Austenitic Stainless Steels at High Temperatures: Processing, Microstructure, Properties and Performance, *Mater. Res.*, 2007, **10**(4), p 453–460